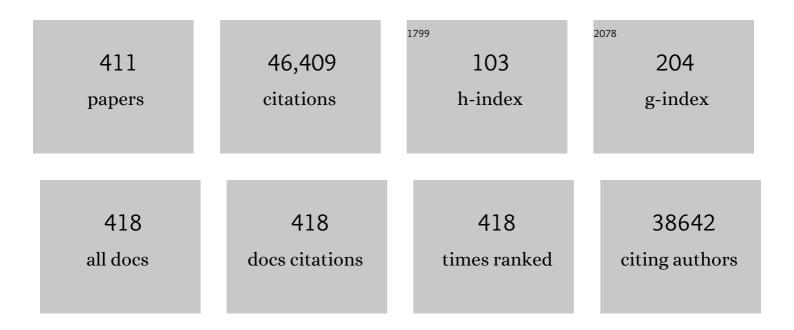
## Michael F Toney

List of Publications by Year in descending order

Source: https://exaly.com/author-pdf/1598997/publications.pdf Version: 2024-02-01



#	Article	IF	CITATIONS
1	Lattice-strain control of the activity in dealloyed core–shell fuel cell catalysts. Nature Chemistry, 2010, 2, 454-460.	13.6	2,489
2	Liquid-crystalline semiconducting polymers with high charge-carrier mobility. Nature Materials, 2006, 5, 328-333.	27.5	2,001
3	A general relationship between disorder, aggregation and charge transport in conjugated polymers. Nature Materials, 2013, 12, 1038-1044.	27.5	1,742
4	Ultra-high mobility transparent organic thin film transistors grown by an off-centre spin-coating method. Nature Communications, 2014, 5, 3005.	12.8	1,155
5	Quantitative Determination of Organic Semiconductor Microstructure from the Molecular to Device Scale. Chemical Reviews, 2012, 112, 5488-5519.	47.7	1,133
6	Dependence of Regioregular Poly(3-hexylthiophene) Film Morphology and Field-Effect Mobility on Molecular Weight. Macromolecules, 2005, 38, 3312-3319.	4.8	1,003
7	Tuning charge transport in solution-sheared organic semiconductors using lattice strain. Nature, 2011, 480, 504-508.	27.8	981
8	Highly oriented crystals at the buried interface in polythiophene thin-film transistors. Nature Materials, 2006, 5, 222-228.	27.5	737
9	Siloxane-Terminated Solubilizing Side Chains: Bringing Conjugated Polymer Backbones Closer and Boosting Hole Mobilities in Thin-Film Transistors. Journal of the American Chemical Society, 2011, 133, 20130-20133.	13.7	628
10	High-Capacity Micrometer-Sized Li <sub>2</sub> S Particles as Cathode Materials for Advanced Rechargeable Lithium-Ion Batteries. Journal of the American Chemical Society, 2012, 134, 15387-15394.	13.7	624
11	Interdiffusion of PCBM and P3HT Reveals Miscibility in a Photovoltaically Active Blend. Advanced Energy Materials, 2011, 1, 82-89.	19.5	572
12	Band Gap Tuning via Lattice Contraction and Octahedral Tilting in Perovskite Materials for Photovoltaics. Journal of the American Chemical Society, 2017, 139, 11117-11124.	13.7	570
13	Voltage-dependent ordering of water molecules at an electrode–electrolyte interface. Nature, 1994, 368, 444-446.	27.8	566
14	Crystalline Ultrasmooth Self-Assembled Monolayers of Alkylsilanes for Organic Field-Effect Transistors. Journal of the American Chemical Society, 2009, 131, 9396-9404.	13.7	562
15	Effects of Thermal Annealing Upon the Morphology of Polymer–Fullerene Blends. Advanced Functional Materials, 2010, 20, 3519-3529.	14.9	539
16	In Operando X-ray Diffraction and Transmission X-ray Microscopy of Lithium Sulfur Batteries. Journal of the American Chemical Society, 2012, 134, 6337-6343.	13.7	475
17	Side-Chain Tunability of Furan-Containing Low-Band-Gap Polymers Provides Control of Structural Order in Efficient Solar Cells. Journal of the American Chemical Society, 2012, 134, 2180-2185.	13.7	458
18	Full open-framework batteries for stationary energy storage. Nature Communications, 2014, 5, 3007.	12.8	440

#	Article	IF	CITATIONS
19	Large modulation of carrier transport by grain-boundary molecular packing and microstructure in organic thin films. Nature Materials, 2009, 8, 952-958.	27.5	416
20	Structural Characterization of a Pentacene Monolayer on an Amorphous SiO2Substrate with Grazing Incidence X-ray Diffraction. Journal of the American Chemical Society, 2004, 126, 4084-4085.	13.7	412
21	The Importance of Fullerene Percolation in the Mixed Regions of Polymer–Fullerene Bulk Heterojunction Solar Cells. Advanced Energy Materials, 2013, 3, 364-374.	19.5	412
22	The Influence of Poly(3-hexylthiophene) Regioregularity on Fullerene-Composite Solar Cell Performance. Journal of the American Chemical Society, 2008, 130, 16324-16329.	13.7	394
23	Bimolecular Crystals of Fullerenes in Conjugated Polymers and the Implications of Molecular Mixing for Solar Cells. Advanced Functional Materials, 2009, 19, 1173-1179.	14.9	392
24	Molecular Packing of High-Mobility Diketo Pyrrolo-Pyrrole Polymer Semiconductors with Branched Alkyl Side Chains. Journal of the American Chemical Society, 2011, 133, 15073-15084.	13.7	381
25	Hybrid Organic–Inorganic Perovskites (HOIPs): Opportunities and Challenges. Advanced Materials, 2015, 27, 5102-5112.	21.0	372
26	High-performance sodium–organic battery by realizing four-sodium storage in disodium rhodizonate. Nature Energy, 2017, 2, 861-868.	39.5	372
27	Direct Observation of Structural Evolution of Metal Chalcogenide in Electrocatalytic Water Oxidation. ACS Nano, 2018, 12, 12369-12379.	14.6	366
28	X-ray Scattering Study of Thin Films of Poly(2,5-bis(3-alkylthiophen-2-yl)thieno[3,2-b]thiophene). Journal of the American Chemical Society, 2007, 129, 3226-3237.	13.7	351
29	Mechanism of Tin Oxidation and Stabilization by Lead Substitution in Tin Halide Perovskites. ACS Energy Letters, 2017, 2, 2159-2165.	17.4	351
30	Compositional and orientational control in metal halide perovskites of reduced dimensionality. Nature Materials, 2018, 17, 900-907.	27.5	351
31	Unconventional Faceâ€On Texture and Exceptional Inâ€Plane Order of a High Mobility nâ€Type Polymer. Advanced Materials, 2010, 22, 4359-4363.	21.0	344
32	The meniscus-guided deposition of semiconducting polymers. Nature Communications, 2018, 9, 534.	12.8	324
33	Critical Role of Side-Chain Attachment Density on the Order and Device Performance of Polythiophenes. Macromolecules, 2007, 40, 7960-7965.	4.8	321
34	Quantification of Thin Film Crystallographic Orientation Using X-ray Diffraction with an Area Detector. Langmuir, 2010, 26, 9146-9151.	3.5	315
35	Chargeâ€Transport Anisotropy Due to Grain Boundaries in Directionally Crystallized Thin Films of Regioregular Poly(3â€hexylthiophene). Advanced Materials, 2009, 21, 1568-1572.	21.0	305
36	Anisotropic Structure and Charge Transport in Highly Strainâ€Aligned Regioregular Poly(3â€hexylthiophene). Advanced Functional Materials, 2011, 21, 3697-3705.	14.9	288

#	Article	IF	CITATIONS
37	Defect-Induced Band-Edge Reconstruction of a Bismuth-Halide Double Perovskite for Visible-Light Absorption. Journal of the American Chemical Society, 2017, 139, 5015-5018.	13.7	288
38	Drastic Control of Texture in a High Performance n-Type Polymeric Semiconductor and Implications for Charge Transport. Macromolecules, 2011, 44, 5246-5255.	4.8	278
39	A map of the inorganic ternary metal nitrides. Nature Materials, 2019, 18, 732-739.	27.5	274
40	Engineering Stress in Perovskite Solar Cells to Improve Stability. Advanced Energy Materials, 2018, 8, 1802139.	19.5	271
41	Quantitative analysis of lattice disorder and crystallite size in organic semiconductor thin films. Physical Review B, 2011, 84, .	3.2	262
42	Molecular Order in High-Efficiency Polymer/Fullerene Bulk Heterojunction Solar Cells. ACS Nano, 2011, 5, 8248-8257.	14.6	260
43	The chemical and structural origin of efficient p-type doping in P3HT. Organic Electronics, 2013, 14, 1330-1336.	2.6	256
44	Chloride in Lead Chloride-Derived Organo-Metal Halides for Perovskite-Absorber Solar Cells. Chemistry of Materials, 2014, 26, 7158-7165.	6.7	256
45	Structural Order in Bulk Heterojunction Films Prepared with Solvent Additives. Advanced Materials, 2011, 23, 2284-2288.	21.0	248
46	Reaction specificity in pyridoxal phosphate enzymes. Archives of Biochemistry and Biophysics, 2005, 433, 279-287.	3.0	246
47	Tuning the Properties of Polymer Bulk Heterojunction Solar Cells by Adjusting Fullerene Size to Control Intercalation. Nano Letters, 2009, 9, 4153-4157.	9.1	243
48	Device-Scale Perpendicular Alignment of Colloidal Nanorods. Nano Letters, 2010, 10, 195-201.	9.1	241
49	The Structure of the Passive Film That Forms on Iron in Aqueous Environments. Journal of the Electrochemical Society, 2000, 147, 2162.	2.9	232
50	The Role of OTS Density on Pentacene and C <sub>60</sub> Nucleation, Thin Film Growth, and Transistor Performance. Advanced Functional Materials, 2009, 19, 1962-1970.	14.9	227
51	Surface regulation enables high stability of single-crystal lithium-ion cathodes at high voltage. Nature Communications, 2020, 11, 3050.	12.8	225
52	Flow-enhanced solution printing of all-polymer solar cells. Nature Communications, 2015, 6, 7955.	12.8	221
53	Observation of Transient Structural-Transformation Dynamics in a Cu <sub>2</sub> S Nanorod. Science, 2011, 333, 206-209.	12.6	220
54	Molecular Characterization of Organic Electronic Films. Advanced Materials, 2011, 23, 319-337.	21.0	215

#	Article	IF	CITATIONS
55	Electrochemical Deposition of Copper on a Gold Electrode in Sulfuric Acid: Resolution of the Interfacial Structure. Physical Review Letters, 1995, 75, 4472-4475.	7.8	213
56	p-Channel Organic Semiconductors Based on Hybrid Aceneâ^'Thiophene Molecules for Thin-Film Transistor Applications. Journal of the American Chemical Society, 2005, 127, 3997-4009.	13.7	204
57	Size-Dependent Lattice Structure and Confinement Properties in CsPbl <sub>3</sub> Perovskite Nanocrystals: Negative Surface Energy for Stabilization. ACS Energy Letters, 2020, 5, 238-247.	17.4	201
58	Ultrafast Growth of Highly Branched Palladium Nanostructures for Catalysis. ACS Nano, 2010, 4, 396-402.	14.6	194
59	Enhanced Solid-State Order and Field-Effect Hole Mobility through Control of Nanoscale Polymer Aggregation. Journal of the American Chemical Society, 2013, 135, 19229-19236.	13.7	194
60	Controlling Solutionâ€Phase Polymer Aggregation with Molecular Weight and Solvent Additives to Optimize Polymerâ€Fullerene Bulk Heterojunction Solar Cells. Advanced Energy Materials, 2014, 4, 1301733.	19.5	194
61	Structure-Activity-Stability Relationships of Ptâ^'Co Alloy Electrocatalysts in Gas-Diffusion Electrode Layers. Journal of Physical Chemistry C, 2007, 111, 3744-3752.	3.1	188
62	Reversible Multivalent (Monovalent, Divalent, Trivalent) Ion Insertion in Open Framework Materials. Advanced Energy Materials, 2015, 5, 1401869.	19.5	185
63	Effect of Al <sub>2</sub> O <sub>3</sub> Coating on Stabilizing LiNi <sub>0.4</sub> Mn <sub>0.4</sub> Co <sub>0.2</sub> O <sub>2</sub> Cathodes. Chemistry of Materials, 2015, 27, 6146-6154.	6.7	185
64	Solid Electrolyte Interphase on Native Oxide-Terminated Silicon Anodes for Li-Ion Batteries. Joule, 2019, 3, 762-781.	24.0	185
65	Impact of Surfaces on Photoinduced Halide Segregation in Mixed-Halide Perovskites. ACS Energy Letters, 2018, 3, 2694-2700.	17.4	184
66	Precise Structure of Pentacene Monolayers on Amorphous Silicon Oxide and Relation to Charge Transport. Advanced Materials, 2009, 21, 2294-2298.	21.0	183
67	Morphologyâ€Dependent Trap Formation in High Performance Polymer Bulk Heterojunction Solar Cells. Advanced Energy Materials, 2011, 1, 954-962.	19.5	183
68	Interfacial Segregation in Polymer/Fullerene Blend Films for Photovoltaic Devices. Macromolecules, 2010, 43, 3828-3836.	4.8	182
69	Structural origin of gap states in semicrystalline polymers and the implications for charge transport. Physical Review B, 2011, 83, .	3.2	180
70	A modular molecular framework for utility in small-molecule solution-processed organic photovoltaic devices. Journal of Materials Chemistry, 2011, 21, 12700.	6.7	175
71	How Nanoparticles Coalesce: An in Situ Study of Au Nanoparticle Aggregation and Grain Growth. Chemistry of Materials, 2011, 23, 3312-3317.	6.7	174
72	Structure of Dealloyed PtCu3Thin Films and Catalytic Activity for Oxygen Reduction. Chemistry of Materials, 2010, 22, 4712-4720.	6.7	173

#	Article	IF	CITATIONS
73	Electrochemical trapping of metastable Mn <sup>3+</sup> ions for activation of MnO <sub>2</sub> oxygen evolution catalysts. Proceedings of the National Academy of Sciences of the United States of America, 2018, 115, E5261-E5268.	7.1	173
74	Surface and grain-boundary scattering in nanometric Cu films. Physical Review B, 2010, 81, .	3.2	172
75	Manipulating the Morphology of P3HT–PCBM Bulk Heterojunction Blends with Solvent Vapor Annealing. Chemistry of Materials, 2012, 24, 3923-3931.	6.7	171
76	Distribution of water molecules at Ag(111)/electrolyte interface as studied with surface X-ray scattering. Surface Science, 1995, 335, 326-332.	1.9	167
77	Crystallization in one-step solution deposition of perovskite films: Upward or downward?. Science Advances, 2021, 7, .	10.3	165
78	Molecular Interactions and Ordering in Electrically Doped Polymers: Blends of PBTTT and F <sub>4</sub> TCNQ. Macromolecules, 2014, 47, 6836-6846.	4.8	164
79	Controlling the Orientation of Terraced Nanoscale "Ribbons―of a Poly(thiophene) Semiconductor. ACS Nano, 2009, 3, 780-787.	14.6	160
80	Activity–stability relationships of ordered and disordered alloy phases of Pt3Co electrocatalysts for the oxygen reduction reaction (ORR). Electrochimica Acta, 2007, 52, 2765-2774.	5.2	159
81	In Situ and Ex Situ Studies of Platinum Nanocrystals: Growth and Evolution in Solution. Journal of the American Chemical Society, 2009, 131, 14590-14595.	13.7	157
82	<i>In Situ</i> X-ray Diffraction Studies of (De)lithiation Mechanism in Silicon Nanowire Anodes. ACS Nano, 2012, 6, 5465-5473.	14.6	156
83	Thermal engineering of FAPbI3 perovskite material via radiative thermal annealing and in situ XRD. Nature Communications, 2017, 8, 14075.	12.8	149
84	Simple Synthesis and Functionalization of Iron Nanoparticles for Magnetic Resonance Imaging. Angewandte Chemie - International Edition, 2011, 50, 4206-4209.	13.8	148
85	Controlling Thin-Film Stress and Wrinkling during Perovskite Film Formation. ACS Energy Letters, 2018, 3, 1225-1232.	17.4	148
86	Controlling reaction specificity in pyridoxal phosphate enzymes. Biochimica Et Biophysica Acta - Proteins and Proteomics, 2011, 1814, 1407-1418.	2.3	145
87	A Mechanistic Understanding of Processing Additiveâ€Induced Efficiency Enhancement in Bulk Heterojunction Organic Solar Cells. Advanced Materials, 2014, 26, 300-305.	21.0	145
88	Fine-Tuning Semiconducting Polymer Self-Aggregation and Crystallinity Enables Optimal Morphology and High-Performance Printed All-Polymer Solar Cells. Journal of the American Chemical Society, 2020, 142, 392-406.	13.7	143
89	Controlling Nucleation and Crystallization in Solutionâ€Processed Organic Semiconductors for Thinâ€Film Transistors. Advanced Materials, 2009, 21, 3605-3609.	21.0	141
90	Synthesis, Alignment, and Magnetic Properties of Monodisperse Nickel Nanocubes. Journal of the American Chemical Society, 2012, 134, 855-858.	13.7	141

#	Article	IF	CITATIONS
91	Molecular Packing and Solar Cell Performance in Blends of Polymers with a Bisadduct Fullerene. Nano Letters, 2012, 12, 1566-1570.	9.1	140
92	Significant dependence of morphology and charge carrier mobility on substrate surface chemistry in high performance polythiophene semiconductor films. Applied Physics Letters, 2007, 90, 062117.	3.3	136
93	Orientational Ordering of Nitrogen Molecular Axes for a Commensurate Monolayer Physisorbed on Graphite. Physical Review Letters, 1982, 48, 177-180.	7.8	130
94	Narrow-Band-Gap Conjugated Chromophores with Extended Molecular Lengths. Journal of the American Chemical Society, 2012, 134, 20609-20612.	13.7	128
95	Structural Origins of Light-Induced Phase Segregation in Organic-Inorganic Halide Perovskite Photovoltaic Materials. Matter, 2020, 2, 207-219.	10.0	128
96	Use of Xâ€Ray Diffraction, Molecular Simulations, and Spectroscopy to Determine the Molecular Packing in a Polymerâ€Fullerene Bimolecular Crystal. Advanced Materials, 2012, 24, 6071-6079.	21.0	126
97	Time-Resolved Structural Evolution of Additive-Processed Bulk Heterojunction Solar Cells. Journal of the American Chemical Society, 2012, 134, 2884-2887.	13.7	125
98	Molecular Basis of Mesophase Ordering in a Thiophene-Based Copolymer. Macromolecules, 2008, 41, 5709-5715.	4.8	114
99	Understanding Phase Transformation in Crystalline Ge Anodes for Li-Ion Batteries. Chemistry of Materials, 2014, 26, 3739-3746.	6.7	112
100	Control of the Electrical Properties in Spinel Oxides by Manipulating the Cation Disorder. Advanced Functional Materials, 2014, 24, 610-618.	14.9	109
101	Three-Dimensional Packing Structure and Electronic Properties of Biaxially Oriented Poly(2,5-bis(3-alkylthiophene-2-yl)thieno[3,2- <i>b</i> ]thiophene) Films. Journal of the American Chemical Society, 2012, 134, 6177-6190.	13.7	108
102	Vertically Segregated Structure and Properties of Small Molecule–Polymer Blend Semiconductors for Organic Thinâ€Film Transistors. Advanced Functional Materials, 2013, 23, 366-376.	14.9	106
103	The formation mechanism for printed silver-contacts for silicon solar cells. Nature Communications, 2016, 7, 11143.	12.8	106
104	The use of poly-cation oxides to lower the temperature of two-step thermochemical water splitting. Energy and Environmental Science, 2018, 11, 2172-2178.	30.8	105
105	Correlating the scattered intensities of P3HT and PCBM to the current densities of polymer solar cells. Chemical Communications, 2011, 47, 436-438.	4.1	103
106	Poly(3-hexylthiophene) and [6,6]-Phenyl-C <sub>61</sub> -butyric Acid Methyl Ester Mixing in Organic Solar Cells. Macromolecules, 2012, 45, 6587-6599.	4.8	103
107	In-situ grazing incidence X-ray diffraction study of electrochemically deposited Pb monolayers on Ag(111). Surface Science, 1988, 193, L29-L36.	1.9	102
108	Versatile Interpenetrating Polymer Network Approach to Robust Stretchable Electronic Devices. Chemistry of Materials, 2017, 29, 7645-7652.	6.7	101

#	Article	IF	CITATIONS
109	Thickness and growth temperature dependence of structure and magnetism in FePt thin films. Journal of Applied Physics, 2003, 93, 9902-9907.	2.5	100
110	Structure and Mechanism of Strength Enhancement in Interpenetrating Polymer Network Hydrogels. Macromolecules, 2011, 44, 5776-5787.	4.8	100
111	Role of confinement and aggregation in charge transport in semicrystalline polythiophene thin films. Physical Review B, 2012, 86, .	3.2	100
112	Real-Time Observation of Poly(3-alkylthiophene) Crystallization and Correlation with Transient Optoelectronic Properties. Macromolecules, 2011, 44, 6653-6658.	4.8	99
113	Aspartate aminotransferase: An old dog teaches new tricks. Archives of Biochemistry and Biophysics, 2014, 544, 119-127.	3.0	99
114	Novel ALD Chemistry Enabled Low-Temperature Synthesis of Lithium Fluoride Coatings for Durable Lithium Anodes. ACS Applied Materials & Interfaces, 2018, 10, 26972-26981.	8.0	99
115	Dominant role of grain boundary scattering in the resistivity of nanometric Cu films. Physical Review B, 2009, 79, .	3.2	98
116	Factors Governing Intercalation of Fullerenes and Other Small Molecules Between the Side Chains of Semiconducting Polymers Used in Solar Cells. Advanced Energy Materials, 2012, 2, 1208-1217.	19.5	97
117	Synthesis, Properties, and Electronic Applications of Size-Controlled Poly(3-hexylthiophene) Nanoparticles. Langmuir, 2010, 26, 13056-13061.	3.5	95
118	Charge Transport in Highly Face-On Poly(3-hexylthiophene) Films. Journal of Physical Chemistry C, 2013, 117, 17421-17428.	3.1	95
119	Emerging In Situ and Operando Nanoscale Xâ€Ray Imaging Techniques for Energy Storage Materials. Advanced Functional Materials, 2015, 25, 1622-1637.	14.9	95
120	Phase, grain structure, stress, and resistivity of sputter-deposited tungsten films. Journal of Vacuum Science and Technology A: Vacuum, Surfaces and Films, 2011, 29, .	2.1	93
121	Effect of Solution Shearing Method on Packing and Disorder of Organic Semiconductor Polymers. Chemistry of Materials, 2015, 27, 2350-2359.	6.7	92
122	Effect of Nonâ€Chlorinated Mixed Solvents on Charge Transport and Morphology of Solutionâ€Processed Polymer Fieldâ€Effect Transistors. Advanced Functional Materials, 2014, 24, 3524-3534.	14.9	89
123	Scalable and Selective Dispersion of Semiconducting Arc-Discharged Carbon Nanotubes by Dithiafulvalene/Thiophene Copolymers for Thin Film Transistors. ACS Nano, 2013, 7, 2659-2668.	14.6	88
124	Confined Interlayer Water Promotes Structural Stability for High-Rate Electrochemical Proton Intercalation in Tungsten Oxide Hydrates. ACS Energy Letters, 2019, 4, 2805-2812.	17.4	88
125	Morphology of Photopolymerized End-Linked Poly(ethylene glycol) Hydrogels by Small-Angle X-ray Scattering. Macromolecules, 2010, 43, 6861-6870.	4.8	87
126	Vertical confinement and interface effects on the microstructure and charge transport of P3HT thin films. Journal of Polymer Science, Part B: Polymer Physics, 2013, 51, 611-620.	2.1	87

#	Article	IF	CITATIONS
127	Ordering Effects in Benzo[1,2â€ <i>b</i> :4,5â€ <i>b</i> ′]difuranâ€thieno[3,4â€ <i>c</i> ]pyrroleâ€4,6â€dione with >7% Solar Cell Efficiency. Advanced Materials, 2014, 26, 4357-4362.	Polymers 21.0	85
128	Spin-Dependent Photovoltaic and Photogalvanic Responses of Optoelectronic Devices Based on Chiral Two-Dimensional Hybrid Organic–Inorganic Perovskites. ACS Nano, 2021, 15, 588-595.	14.6	85
129	Interplay between Energetic and Kinetic Factors on the Ambient Stability of n-Channel Organic Transistors Based on Perylene Diimide Derivatives. Chemistry of Materials, 2009, 21, 5508-5518.	6.7	84
130	Thiophene-rich fused-aromatic thienopyrazine acceptor for donor–acceptor low band-gap polymers for OTFT and polymer solar cell applications. Journal of Materials Chemistry, 2010, 20, 5823.	6.7	84
131	In situ measurement of power conversion efficiency and molecular ordering during thermal annealing in P3HT:PCBM bulk heterojunction solar cells. Journal of Materials Chemistry, 2011, 21, 15224.	6.7	84
132	Electrochemical ion insertion from the atomic to the device scale. Nature Reviews Materials, 2021, 6, 847-867.	48.7	84
133	Origin of low-friction behavior in graphite investigated by surface x-ray diffraction. Applied Physics Letters, 2004, 84, 4702-4704.	3.3	83
134	A Supramolecular Complex in Smallâ€Molecule Solar Cells based on Contorted Aromatic Molecules. Angewandte Chemie - International Edition, 2012, 51, 8594-8597.	13.8	82
135	Effects of Odd–Even Side Chain Length of Alkyl-Substituted Diphenylbithiophenes on First Monolayer Thin Film Packing Structure. Journal of the American Chemical Society, 2013, 135, 11006-11014.	13.7	81
136	Acoustic phonon lifetimes limit thermal transport in methylammonium lead iodide. Proceedings of the National Academy of Sciences of the United States of America, 2018, 115, 11905-11910.	7.1	81
137	Observation of the effect of refraction on x rays diffracted in a grazing-incidence asymmetric Bragg geometry. Physical Review B, 1989, 39, 7963-7966.	3.2	80
138	Laser-Synthesized Epitaxial Graphene. ACS Nano, 2010, 4, 7524-7530.	14.6	79
139	Electron mean free path of tungsten and the electrical resistivity of epitaxial (110) tungsten films. Physical Review B, 2012, 86, .	3.2	79
140	Particle size effect of hydrogen-induced lattice expansion of palladium nanoclusters. Physical Review B, 2008, 78, .	3.2	78
141	Structural Characterization of Vapor-Deposited Glasses of an Organic Hole Transport Material with X-ray Scattering. Chemistry of Materials, 2015, 27, 3341-3348.	6.7	78
142	Mechanistic Studies on Sintering of Silver Nanoparticles. Chemistry of Materials, 2011, 23, 4634-4640.	6.7	77
143	Effects of Confinement on Microstructure and Charge Transport in High Performance Semicrystalline Polymer Semiconductors. Advanced Functional Materials, 2013, 23, 2091-2098.	14.9	77
144	Morphological Origin of Charge Transport Anisotropy in Aligned Polythiophene Thin Films. Advanced Functional Materials, 2014, 24, 3422-3431.	14.9	77

#	Article	IF	CITATIONS
145	Transformation from crystalline precursor to perovskite in PbCl2-derived MAPbI3. Nature Communications, 2018, 9, 3458.	12.8	77
146	Solid‣tate Supramolecular Organization of Polythiophene Chains Containing Thienothiophene Units. Advanced Materials, 2009, 21, 1193-1198.	21.0	76
147	Effect of Backbone Regioregularity on the Structure and Orientation of a Donor–Acceptor Semiconducting Copolymer. Macromolecules, 2014, 47, 1403-1410.	4.8	76
148	NASICON Na <sub>3</sub> V <sub>2</sub> (PO <sub>4</sub> ) <sub>3</sub> Enables Quasi-Two-Stage Na <sup>+</sup> and Zn <sup>2+</sup> Intercalation for Multivalent Zinc Batteries. Chemistry of Materials, 2020, 32, 3028-3035.	6.7	75
149	Beyond Local Solvation Structure: Nanometric Aggregates in Battery Electrolytes and Their Effect on Electrolyte Properties. ACS Energy Letters, 2022, 7, 461-470.	17.4	75
150	Correlating the microstructure of thin films of poly[5,5-bis(3-dodecyl-2-thienyl)-2,2-bithiophene] with charge transport: Effect of dielectric surface energy and thermal annealing. Physical Review B, 2008, 78, .	3.2	74
151	Photovoltaic Universal Joints: Ballâ€andâ€Socket Interfaces in Molecular Photovoltaic Cells. ChemPhysChem, 2010, 11, 799-803.	2.1	74
152	Comparison of the Photovoltaic Characteristics and Nanostructure of Fullerenes Blended with Conjugated Polymers with Siloxane-Terminated and Branched Aliphatic Side Chains. Chemistry of Materials, 2013, 25, 431-440.	6.7	74
153	Underpotentially deposited thallium on silver (111) byin situsurface x-ray scattering. Physical Review B, 1992, 45, 9362-9374.	3.2	73
154	Measurements of carbon thin films using xâ€ray reflectivity. Journal of Applied Physics, 1989, 66, 1861-1863.	2.5	72
155	Molecular design for improved photovoltaic efficiency: band gap and absorption coefficient engineering. Journal of Materials Chemistry, 2009, 19, 7195.	6.7	72
156	Can Polymorphism be Used to form Branched Metal Nanostructures?. Advanced Materials, 2013, 25, 1552-1556.	21.0	72
157	Size and composition distribution dynamics of alloy nanoparticle electrocatalysts probed by anomalous small angle X-ray scattering (ASAXS). Faraday Discussions, 2008, 140, 283-296.	3.2	71
158	The phase behavior of a polymerâ€fullerene bulk heterojunction system that contains bimolecular crystals. Journal of Polymer Science, Part B: Polymer Physics, 2011, 49, 499-503.	2.1	71
159	Emerging X-ray imaging technologies for energy materials. Materials Today, 2020, 34, 132-147.	14.2	70
160	Small-Molecule Thiophene-C <sub>60</sub> Dyads As Compatibilizers in Inverted Polymer Solar Cells. Chemistry of Materials, 2010, 22, 5762-5773.	6.7	68
161	Effect of Surfactant Concentration and Aggregation on the Growth Kinetics of Nickel Nanoparticles. Journal of Physical Chemistry C, 2013, 117, 16709-16718.	3.1	68
162	Controlling the Microstructure of Solution-Processable Small Molecules in Thin-Film Transistors through Substrate Chemistry. Chemistry of Materials, 2011, 23, 1194-1203.	6.7	67

#	Article	IF	CITATIONS
163	3,4-Disubstituted Polyalkylthiophenes for High-Performance Thin-Film Transistors and Photovoltaics. Journal of the American Chemical Society, 2011, 133, 16722-16725.	13.7	67
164	Surface x-ray-scattering measurements of the substrate-induced spatial modulation of an incommensurate adsorbed monolayer. Physical Review B, 1990, 42, 5594-5603.	3.2	66
165	Effects of the surface roughness of plastic-compatible inorganic dielectrics on polymeric thin film transistors. Applied Physics Letters, 2007, 90, 233508.	3.3	66
166	Mechanism of Crystallization and Implications for Charge Transport in Poly(3â€ethylhexylthiophene) Thin Films. Advanced Functional Materials, 2014, 24, 4515-4521.	14.9	66
167	Crystallizationâ€Induced Phase Separation in Solutionâ€Processed Small Molecule Bulk Heterojunction Organic Solar Cells. Advanced Functional Materials, 2014, 24, 3543-3550.	14.9	66
168	General Post-annealing Method Enables High-Efficiency Two-Dimensional Perovskite Solar Cells. ACS Applied Materials & Interfaces, 2018, 10, 33187-33197.	8.0	66
169	Thin Film Structure of Tetraceno[2,3- <i>b</i> ]thiophene Characterized by Grazing Incidence X-ray Scattering and Near-Edge X-ray Absorption Fine Structure Analysis. Journal of the American Chemical Society, 2008, 130, 3502-3508.	13.7	65
170	Dealloying of Cu <sub>3</sub> Pt (111) Studied by Surface X-ray Scattering. Journal of Physical Chemistry C, 2011, 115, 9074-9080.	3.1	65
171	Structural and Rheological Properties of Meibomian Lipid. , 2013, 54, 2720.		63
172	Low-energy electron diffraction study of molecular oxygen physisorbed on graphite. Physical Review B, 1987, 36, 1248-1258.	3.2	62
173	Influence of Surfactant Structure on Reverse Micelle Size and Charge for Nonpolar Electrophoretic Inks. Langmuir, 2011, 27, 11845-11851.	3.5	62
174	Correlating photovoltaic properties of a PTB7-Th:PC <sub>71</sub> BM blend to photophysics and microstructure as a function of thermal annealing. Journal of Materials Chemistry A, 2017, 5, 14646-14657.	10.3	61
175	In Situ Observation of Strain Development and Porosity Evolution in Nanoporous Gold Foils. Advanced Functional Materials, 2011, 21, 3938-3946.	14.9	60
176	Engineering Amyloid Fibrils from β-Solenoid Proteins for Biomaterials Applications. ACS Nano, 2015, 9, 449-463.	14.6	60
177	Zone-Refinement Effect in Small Moleculeâ ´Polymer Blend Semiconductors for Organic Thin-Film Transistors. Journal of the American Chemical Society, 2011, 133, 412-415.	13.7	59
178	The Role of Solvent Additive Processing in High Performance Small Molecule Solar Cells. Chemistry of Materials, 2014, 26, 6531-6541.	6.7	58
179	Tuning the bandgap of Cs <sub>2</sub> AgBiBr <sub>6</sub> through dilute tin alloying. Chemical Science, 2019, 10, 10620-10628.	7.4	58
180	Quantification of heterogeneous, irreversible lithium plating in extreme fast charging of lithium-ion batteries. Energy and Environmental Science, 2021, 14, 4979-4988.	30.8	58

#	Article	IF	CITATIONS
181	Rotational epitaxy of a nontriangular structure: Thel´phase of oxygen physisorbed on graphite. Physical Review B, 1983, 27, 6413-6417.	3.2	57
182	Angle-resolved photoemission and quasiparticle calculation of ZnO: The need for <mml:math xmlns:mml="http://www.w3.org/1998/Math/MathML" display="inline"&gt;<mml:mi>d</mml:mi>band shift in oxide semiconductors. Physical Review B, 2012, 86, .</mml:math 	3.2	56
183	Sequentially solution-processed, nanostructured polymer photovoltaics using selective solvents. Energy and Environmental Science, 2014, 7, 1103.	30.8	56
184	High-fraction brookite films from amorphous precursors. Scientific Reports, 2017, 7, 15232.	3.3	56
185	Tuning the Morphology of All-Polymer OPVs through Altering Polymer–Solvent Interactions. Chemistry of Materials, 2014, 26, 5020-5027.	6.7	54
186	Controlling the Texture and Crystallinity of Evaporated Lead Phthalocyanine Thin Films for Near-Infrared Sensitive Solar Cells. ACS Applied Materials & Interfaces, 2013, 5, 8505-8515.	8.0	53
187	Ultrafast Electron Transfer at Organic Semiconductor Interfaces: Importance of Molecular Orientation. Journal of Physical Chemistry Letters, 2015, 6, 6-12.	4.6	52
188	Water-in-Salt LiTFSI Aqueous Electrolytes. 1. Liquid Structure from Combined Molecular Dynamics Simulation and Experimental Studies. Journal of Physical Chemistry B, 2021, 125, 4501-4513.	2.6	52
189	High efficiency amine functionalization of cycloolefin polymer surfaces for biodiagnostics. Journal of Materials Chemistry, 2010, 20, 4116.	6.7	51
190	Temperature-Induced Transitions in the Structure and Interfacial Rheology of Human Meibum. Biophysical Journal, 2012, 102, 369-376.	0.5	51
191	Storage Capacity and Cycling Stability in Ge Anodes: Relationship of Anode Structure and Cycling Rate. Advanced Energy Materials, 2015, 5, 1500599.	19.5	51
192	Coverage effects on the magnetism ofFeâ^•MgO(001)ultrathin films. Physical Review B, 2005, 71, .	3.2	50
193	Dealloyed PdCu3 thin film electrocatalysts for oxygen reduction reaction. Journal of Power Sources, 2013, 222, 169-176.	7.8	50
194	Humidity-Induced Photoluminescence Hysteresis in Variable Cs/Br Ratio Hybrid Perovskites. Journal of Physical Chemistry Letters, 2018, 9, 3463-3469.	4.6	50
195	Cross-Linked Ultrathin Polyurea Films via Molecular Layer Deposition. Macromolecules, 2013, 46, 5638-5643.	4.8	49
196	Origin of Anisotropic Molecular Packing in Vapor-Deposited Alq3 Glasses. Journal of Physical Chemistry Letters, 2019, 10, 164-170.	4.6	49
197	Heterogeneous Behavior of Lithium Plating during Extreme Fast Charging. Cell Reports Physical Science, 2020, 1, 100114.	5.6	49
198	Low-energy electron diffraction determination of the structure of theζphase of oxygen physisorbed on graphite. Physical Review B, 1984, 30, 1115-1118.	3.2	48

#	Article	IF	CITATIONS
199	Thickness Measurements of Thin Perfluoropolyether Polymer Films on Silicon and Amorphous-Hydrogenated Carbon with X-Ray Reflectivity, ESCA and Optical Ellipsometry. Journal of Colloid and Interface Science, 2000, 225, 219-226.	9.4	47
200	Measuring Domain Sizes and Compositional Heterogeneities in P3HTâ€PCBM Bulk Heterojunction Thin Films with <sup>1</sup> H Spin Diffusion NMR Spectroscopy. Advanced Functional Materials, 2012, 22, 1255-1266.	14.9	47
201	Rapid fabrication of a novel Sn–Ge alloy: structure–property relationship and its enhanced lithium storage properties. Journal of Materials Chemistry A, 2013, 1, 14577.	10.3	47
202	Thermal annealing study of exchangeâ€biased NiFeâ€FeMn films. Journal of Applied Physics, 1991, 70, 6227-6229.	2.5	46
203	A Quantitative Correlation between the Mobility and Crystallinity of Photo-Cross-Linkable P3HT. Macromolecules, 2012, 45, 3057-3062.	4.8	46
204	The nanoscale structure of the electrolyte–metal oxide interface. Energy and Environmental Science, 2018, 11, 594-602.	30.8	46
205	Reversible Soft-Contact Lamination and Delamination for Non-Invasive Fabrication and Characterization of Bulk-Heterojunction and Bilayer Organic Solar Cells. Chemistry of Materials, 2010, 22, 4931-4938.	6.7	45
206	Water or Anion? Uncovering the Zn <sup>2+</sup> Solvation Environment in Mixed Zn(TFSI) <sub>2</sub> and LiTFSI Water-in-Salt Electrolytes. ACS Energy Letters, 2021, 6, 3458-3463.	17.4	45
207	Heavy-Enzyme Kinetic Isotope Effects on Proton Transfer in Alanine Racemase. Journal of the American Chemical Society, 2013, 135, 2509-2511.	13.7	44
208	A simple droplet pinning method for polymer film deposition for measuring charge transport in a thin film transistor. Organic Electronics, 2012, 13, 2450-2460.	2.6	43
209	Use of a commercially available nucleating agent to control the morphological development of solution-processed small molecule bulk heterojunction organic solar cells. Journal of Materials Chemistry A, 2014, 2, 15717-15721.	10.3	43
210	Crystalline Structure in Thin Films of DEHâ^'PPV Homopolymer and PPV-b-PI Rodâ^'Coil Block Copolymers. Macromolecules, 2008, 41, 58-66.	4.8	42
211	Influence of substrate on crystallization in polythiophene/fullerene blends. Solar Energy Materials and Solar Cells, 2011, 95, 1375-1381.	6.2	42
212	Molecular Structure of Interfacial Human Meibum Films. Langmuir, 2012, 28, 11858-11865.	3.5	42
213	Fluoroethylene Carbonate Induces Ordered Electrolyte Interface on Silicon and Sapphire Surfaces as Revealed by Sum Frequency Generation Vibrational Spectroscopy and X-ray Reflectivity. Nano Letters, 2018, 18, 2105-2111.	9.1	42
214	Donor Conjugated Polymers with Polar Side Chain Groups: The Role of Dielectric Constant and Energetic Disorder on Photovoltaic Performance. Advanced Functional Materials, 2018, 28, 1803418.	14.9	42
215	Preferred crystallographic orientation of cellulose in plant primary cell walls. Nature Communications, 2020, 11, 4720.	12.8	41
216	Microstructure and properties of ultrathin amorphous silicon nitride protective coating. Journal of Vacuum Science and Technology A: Vacuum, Surfaces and Films, 2003, 21, 1895-1904.	2.1	40

#	Article	IF	CITATIONS
217	Strain development in nanoporous metallic foils formed by dealloying. Applied Physics Letters, 2008, 92, .	3.3	40
218	Inducing Molecular Aggregation of Polymer Semiconductors in a Secondary Insulating Polymer Matrix to Enhance Charge Transport. Chemistry of Materials, 2020, 32, 897-905.	6.7	40
219	Thickness dependence of exchange bias and structure in MnPt and MnNi spin valves. Applied Physics Letters, 2002, 81, 4565-4567.	3.3	39
220	Tuning Contact Recombination and Open-Circuit Voltage in Polymer Solar Cells via Self-Assembled Monolayer Adsorption at the Organic–Metal Oxide Interface. Journal of Physical Chemistry C, 2013, 117, 20474-20484.	3.1	39
221	The Atomic Scale Electrochemical Lithiation and Delithiation Process of Silicon. Advanced Materials Interfaces, 2017, 4, 1700771.	3.7	39
222	Impact of Processing on Structural and Compositional Evolution in Mixed Metal Halide Perovskites during Film Formation. Advanced Functional Materials, 2020, 30, 2001752.	14.9	39
223	Toward Unraveling the Origin of Lithium Fluoride in the Solid Electrolyte Interphase. Chemistry of Materials, 2021, 33, 7315-7336.	6.7	39
224	Solutionâ€Processed Nanostructured Benzoporphyrin with Polycarbonate Binder for Photovoltaics. Advanced Materials, 2011, 23, 2289-2293.	21.0	38
225	Impact of Polymer Side Chain Modification on OPV Morphology and Performance. Chemistry of Materials, 2018, 30, 7872-7884.	6.7	38
226	Sulfur-Donor Solvents Strongly Coordinate Pb <sup>2+</sup> in Hybrid Organic–Inorganic Perovskite Precursor Solutions. Journal of Physical Chemistry C, 2020, 124, 14496-14502.	3.1	38
227	Morphological, Chemical, and Electronic Changes of the Conjugated Polymer PTB7 with Thermal Annealing. IScience, 2018, 2, 182-192.	4.1	37
228	Computational Studies on Nonenzymatic and Enzymatic Pyridoxal Phosphate Catalyzed Decarboxylations of 2-Aminoisobutyrateâ€. Biochemistry, 2001, 40, 1378-1384.	2.5	36
229	Dependence of Crystallite Formation and Preferential Backbone Orientations on the Side Chain Pattern in PBDTTPD Polymers. ACS Applied Materials & Interfaces, 2014, 6, 19477-19481.	8.0	36
230	Microstructure of Oligofluorene Asymmetric Derivatives in Organic Thin Film Transistors. Chemistry of Materials, 2008, 20, 2763-2772.	6.7	35
231	Self-Doping and Electrical Conductivity in Spinel Oxides: Experimental Validation of Doping Rules. Chemistry of Materials, 2014, 26, 1867-1873.	6.7	35
232	Radiative Thermal Annealing/in Situ X-ray Diffraction Study of Methylammonium Lead Triiodide: Effect of Antisolvent, Humidity, Annealing Temperature Profile, and Film Substrates. Chemistry of Materials, 2017, 29, 5931-5941.	6.7	35
233	Stoichiometry–anisotropy connections in epitaxial L10 FePt(001) films. Journal of Applied Physics, 2004, 95, 7501-7503.	2.5	34
234	Fabrication of organic semiconductor crystalline thin films and crystals from solution by confined crystallization. Organic Electronics, 2012, 13, 235-243.	2.6	34

#	Article	IF	CITATIONS
235	Negative-pressure polymorphs made by heterostructural alloying. Science Advances, 2018, 4, eaaq1442.	10.3	34
236	FA <sub><i>x</i></sub> Cs <sub>1–<i>x</i></sub> PbI <sub>3</sub> Nanocrystals: Tuning Crystal Symmetry by A-Site Cation Composition. ACS Energy Letters, 2020, 5, 2475-2482.	17.4	34
237	Vapor-Deposited Glass Structure Determined by Deposition Rate–Substrate Temperature Superposition Principle. Journal of Physical Chemistry Letters, 2019, 10, 3536-3542.	4.6	33
238	Stable solvent for solution-based electrical doping of semiconducting polymer films and its application to organic solar cells. Energy and Environmental Science, 2018, 11, 2216-2224.	30.8	32
239	Achieving High Thermoelectric Performance and Metallic Transport in Solventâ€Sheared PEDOT:PSS. Advanced Electronic Materials, 2021, 7, 2001190.	5.1	32
240	Side chain engineering of fused aromatic thienopyrazine based low band-gap polymers for enhanced charge carrier mobility. Journal of Materials Chemistry, 2011, 21, 1537-1543.	6.7	30
241	Vapor deposition of a nonmesogen prepares highly structured organic glasses. Proceedings of the National Academy of Sciences of the United States of America, 2019, 116, 21421-21426.	7.1	30
242	Structural depth profiling of iron oxide thin films using grazing incidence asymmetric Bragg xâ€fay diffraction. Journal of Applied Physics, 1989, 65, 4763-4768.	2.5	29
243	Solution-Processable α,ï‰-Distyryl Oligothiophene Semiconductors with Enhanced Environmental Stability. Chemistry of Materials, 2009, 21, 1927-1938.	6.7	29
244	Coulombically-stabilized oxygen hole polarons enable fully reversible oxygen redox. Energy and Environmental Science, 2021, 14, 4858-4867.	30.8	29
245	Synthesis and Characterization of K <sub>8â^²<i>xx</i></sub> (H <sub>2</sub> ) <sub><i>y</i></sub> Si <sub>46</sub> . Inorganic Chemistry, 2010, 49, 815-822.	4.0	28
246	Identifying and managing radiation damage during in situ transmission x-ray microscopy of Li-ion batteries. Proceedings of SPIE, 2013, , .	0.8	28
247	Impact of Hole Transport Layer Surface Properties on the Morphology of a Polymerâ€Fullerene Bulk Heterojunction. Advanced Energy Materials, 2014, 4, 1301879.	19.5	28
248	The Crystalline Structure of Copper Phthalocyanine Films on ZnO(11Ì00). Journal of the American Chemical Society, 2012, 134, 14302-14305.	13.7	27
249	Growth Trajectories and Coarsening Mechanisms of Metal Nanoparticle Electrocatalysts. ChemCatChem, 2012, 4, 766-770.	3.7	27
250	Ultrathin Body Poly(3-hexylthiophene) Transistors with Improved Short-Channel Performance. ACS Applied Materials & Interfaces, 2013, 5, 2342-2346.	8.0	27
251	Spectromicroscopy and coherent diffraction imaging: focus on energy materials applications. Journal of Synchrotron Radiation, 2014, 21, 1019-1030.	2.4	27
252	Enhancing Molecular Alignment and Charge Transport of Solutionâ€Sheared Semiconducting Polymer Films by the Electricalâ€Blade Effect. Advanced Electronic Materials, 2018, 4, 1800110.	5.1	27

#	Article	IF	CITATIONS
253	Mechanism of Additive-Assisted Room-Temperature Processing of Metal Halide Perovskite Thin Films. ACS Applied Materials & Interfaces, 2021, 13, 13212-13225.	8.0	27
254	Influence of Annealing and Composition on the Crystal Structure of Mixed-Halide, Ruddlesden–Popper Perovskites. Chemistry of Materials, 2022, 34, 3109-3122.	6.7	27
255	Understanding additive controlled lithium morphology in lithium metal batteries. Journal of Materials Chemistry A, 2020, 8, 16960-16972.	10.3	26
256	Degradation mechanisms in mixed-cation and mixed-halide Cs <sub>x</sub> FA <sub>1â^'x</sub> Pb(Br <sub>y</sub> 1s^'y) <sub>3</sub> perovskite films under ambient conditions. Journal of Materials Chemistry A, 2020, 8, 9302-9312.	10.3	26
257	Clipped Random Wave Morphologies and the Analysis of the SAXS of an Ionomer Formed by Copolymerization of Tetrafluoroethylene and CF2â•CFO(CF2)4SO3H. Macromolecules, 2009, 42, Asyminetric cation nonstoichiometry in spinels: Site occupancy in Co <mml:math< td=""><td>4.8</td><td>25</td></mml:math<>	4.8	25
258	xmlns:mml="http://www.w3.org/1998/Math/MathML" display="inline"> <mml:msub><mml:mrow /&gt;<mml:mn>2</mml:mn></mml:mrow </mml:msub> ZnO <mml:math xmlns:mml="http://www.w3.org/1998/Math/MathML" display="inline"&gt;<mml:msub><mml:mrow /&gt;<mml:mn>4</mml:mn></mml:mrow </mml:msub>and Rh<mml:math xmlns:mml="http://www.w3.org/1998/Math/MathML" display="inline"&gt;<mml:msub><mml:mrow< td=""><td>3.2</td><td>25</td></mml:mrow<></mml:msub></mml:math </mml:math 	3.2	25
259	Substrate-Induced Variations of Molecular Packing, Dynamics, and Intermolecular Electronic Couplings in Pentacene Monolayers on the Amorphous Silica Dielectric. ACS Nano, 2014, 8, 690-700.	14.6	25
260	Vapor-Deposited Glasses with Long-Range Columnar Liquid Crystalline Order. Chemistry of Materials, 2017, 29, 9110-9119.	6.7	25
261	Shedding X-ray Light on the Interfacial Electrochemistry of Silicon Anodes for Li-Ion Batteries. Accounts of Chemical Research, 2019, 52, 2673-2683.	15.6	25
262	Toward quantifying capacity losses due to solid electrolyte interphase evolution in silicon thin film batteries. Journal of Chemical Physics, 2020, 152, 084702.	3.0	25
263	Structural properties of epitaxial SrHfO3 thin films on Si (001). Thin Solid Films, 2010, 518, S118-S122.	1.8	24
264	Chemical Annealing of Zinc Tetraphenylporphyrin Films: Effects on Film Morphology and Organic Photovoltaic Performance. Chemistry of Materials, 2012, 24, 2583-2591.	6.7	24
265	Solution-Phase Conformation and Dynamics of Conjugated Isoindigo-Based Donor–Acceptor Polymer Single Chains. Journal of Physical Chemistry Letters, 2017, 8, 5479-5486.	4.6	24
266	Tuning Intra and Intermolecular Interactions for Balanced Hole and Electron Transport in Semiconducting Polymers. Chemistry of Materials, 2020, 32, 7338-7346.	6.7	24
267	Alloying a single and a double perovskite: a Cu <sup>+/2+</sup> mixed-valence layered halide perovskite with strong optical absorption. Chemical Science, 2021, 12, 8689-8697.	7.4	24
268	Structural effect of PtRu–WO3 alloy nanostructures on methanol electrooxidation. Electrochemistry Communications, 2006, 8, 359-363.	4.7	23
269	Thin Film Transistors Based on Alkylphenyl Quaterthiophenes:Â Structure and Electrical Transport Properties. Chemistry of Materials, 2007, 19, 1355-1361.	6.7	23
270	Insertion Mechanism of a Poly(ethylene oxide)-poly(butylene oxide) Block Copolymer into a DPPC Monolayer. Langmuir, 2011, 27, 11444-11450.	3.5	23

#	Article	IF	CITATIONS
271	Tuning crystalline ordering by annealing and additives to study its effect on exciton diffusion in a polyalkylthiophene copolymer. Physical Chemistry Chemical Physics, 2017, 19, 12441-12451.	2.8	23
272	High-capacity thermochemical CO <sub>2</sub> dissociation using iron-poor ferrites. Energy and Environmental Science, 2020, 13, 592-600.	30.8	23
273	Mixing Matters: Nanoscale Heterogeneity and Stability in Metal Halide Perovskite Solar Cells. ACS Energy Letters, 2022, 7, 471-480.	17.4	23
274	Probing the effect of substrate heating during deposition of DCV4T:C60 blend layers for organic solar cells. Organic Electronics, 2012, 13, 623-631.	2.6	22
275	Synthesis, solidâ€state, and chargeâ€transport properties of conjugated polythiopheneâ€ <i>S</i> , <i>S</i> â€dioxides. Journal of Polymer Science, Part B: Polymer Physics, 2013, 51, 48-56.	2.1	22
276	Engineering epitaxial γ-Al2O3 gate dielectric films on 4H-SiC. Journal of Applied Physics, 2007, 102, 104112.	2.5	21
277	Improved Efficiency in Poly(3-hexylthiophene)/Zinc Oxide Solar Cells via Lithium Incorporation. Journal of Physical Chemistry C, 2009, 113, 17608-17612.	3.1	21
278	Janus: Prediction and Ranking of Mutations Required for Functional Interconversion of Enzymes. Journal of Molecular Biology, 2013, 425, 1378-1389.	4.2	21
279	Two-Dimensional GIWAXS Reveals a Transient Crystal Phase in Solution-Processed Thermally Converted Tetrabenzoporphyrin. Journal of Physical Chemistry B, 2013, 117, 14557-14567.	2.6	21
280	Operando Spectromicroscopy of Sulfur Species in Lithium-Sulfur Batteries. Journal of the Electrochemical Society, 2018, 165, A6043-A6050.	2.9	21
281	Microstructural Evolution of the Thin Films of a Donor–Acceptor Semiconducting Polymer Deposited by Meniscus-Guided Coating. Macromolecules, 2018, 51, 4325-4340.	4.8	21
282	Bridging the thermodynamics and kinetics of temperature-induced morphology evolution in polymer/fullerene organic solar cell bulk heterojunction. Materials Horizons, 2021, 8, 1272-1285.	12.2	21
283	Extraction of pore-morphology and capillary pressure curves of porous media from synchrotron-based tomography data. Scientific Reports, 2015, 5, 10635.	3.3	20
284	Synthesis of Poly(bisisoindigo) Using a Metal-Free Aldol Polymerization for Thin-Film Transistor Applications. ACS Applied Materials & Interfaces, 2020, 12, 14265-14271.	8.0	20
285	Compositional heterogeneity in Cs <sub><i>y</i></sub> FA <sub>1â<sup>°</sup> <i>y</i></sub> Pb(Br <sub><i>x</i></sub> I <sub>1â<sup>°</sup> <i>x</i></sub> ) <sub>3 perovskite films and its impact on phase behavior. Energy and Environmental Science, 2021, 14, 6394-6405.</sub>	'sub≻ 30.8	20
286	Unraveling the Unconventional Order of a High-Mobility Indacenodithiophene–Benzothiadiazole Copolymer. ACS Macro Letters, 2021, 10, 1306-1314.	4.8	20
287	Comment on â€~â€~Superstructures of Pb monolayers electrochemically deposited on Ag(111)''. Physical Review B, 1994, 49, 7793-7794.	3.2	19
288	Synthesis of regioregular pentacene-containing conjugated polymers. Journal of Materials Chemistry, 2011, 21, 7078.	6.7	19

#	Article	IF	CITATIONS
289	Behaviors of Fe, Zn, and Ga Substitution in CulnS <sub>2</sub> Nanoparticles Probed with Anomalous X-ray Diffraction. Chemistry of Materials, 2013, 25, 320-325.	6.7	19
290	Registration of the rotation axis in X-ray tomography. Journal of Synchrotron Radiation, 2015, 22, 452-457.	2.4	19
291	Using heterostructural alloying to tune the structure and properties of the thermoelectric Sn <sub>1â^'x</sub> Ca <sub>x</sub> Se. Journal of Materials Chemistry A, 2017, 5, 16873-16882.	10.3	19
292	Molecular Orientation for Vapor-Deposited Organic Glasses Follows Rate-Temperature Superposition: The Case of Posaconazole. Journal of Physical Chemistry B, 2020, 124, 2505-2513.	2.6	19
293	Modular construction of P3HT/PCBM planar-heterojunction solar cells by lamination allows elucidation of processing–structure–function relationships. Organic Electronics, 2011, 12, 1963-1972.	2.6	18
294	Exploring the influence of iron substitution in lithium rich layered oxides Li <sub>2</sub> Ru <sub>1â^'x</sub> Fe <sub>x</sub> O <sub>3</sub> : triggering the anionic redox reaction. Journal of Materials Chemistry A, 2017, 5, 14387-14396.	10.3	18
295	Synthesis of Polycrystalline Ruddlesden–Popper Organic Lead Halides and Their Growth Dynamics. Chemistry of Materials, 2019, 31, 9472-9479.	6.7	18
296	Melting of Magnesium Borohydride under High Hydrogen Pressure: Thermodynamic Stability and Effects of Nanoconfinement. Chemistry of Materials, 2020, 32, 5604-5615.	6.7	18
297	High anisotropy CoPtCrB magnetic recording media. Journal of Applied Physics, 2003, 94, 4018-4023.	2.5	17
298	Pore Morphologies in Disordered Nanoporous Thin Films. Langmuir, 2004, 20, 1535-1538.	3.5	17
299	Effects of Thermal Annealing Upon the Nanomorphology of Poly(3â€hexylselenophene)â€PCBM Blends. Macromolecular Rapid Communications, 2011, 32, 1454-1460.	3.9	17
300	Efficient Energy Sensitization of C <sub>60</sub> and Application to Organic Photovoltaics. Journal of the American Chemical Society, 2013, 135, 11920-11928.	13.7	17
301	Langmuir–Blodgett Thin Films of Diketopyrrolopyrrole-Based Amphiphiles. ACS Applied Materials & Interfaces, 2018, 10, 11995-12004.	8.0	17
302	RNA binding candidates for human ADAR3 from substrates of a gain of function mutant expressed in neuronal cells. Nucleic Acids Research, 2019, 47, 10801-10814.	14.5	17
303	Using Deposition Rate and Substrate Temperature to Manipulate Liquid Crystal-Like Order in a Vapor-Deposited Hexagonal Columnar Glass. Journal of Physical Chemistry B, 2021, 125, 2761-2770.	2.6	17
304	Quantification of Efficiency in Lithium Metal Negative Electrodes via Operando X-ray Diffraction. Chemistry of Materials, 2021, 33, 7537-7545.	6.7	17
305	Structure and epitaxy of anodic TiO2/Ti(110). Surface Science, 1992, 268, 57-72.	1.9	16
306	5,11-Conjugation-extended low-bandgap anthradithiophene-containing polymer exhibiting enhanced thin-film order and field-effect mobility. Chemical Communications, 2012, 48, 7286.	4.1	16

#	Article	IF	CITATIONS
307	Nitrate reductase 15N discrimination in Arabidopsis thaliana, Zea mays, Aspergillus niger, Pichea angusta, and Escherichia coli. Frontiers in Plant Science, 2014, 5, 317.	3.6	16
308	Structural properties of epitaxial γ-Al2O3 (111) thin films on 4H-SiC (0001). Applied Physics Letters, 2007, 90, 061916.	3.3	15
309	Langmuir Monolayers of Straight-Chain and Branched Hexadecanol and Eicosanol Mixtures. Langmuir, 2008, 24, 14005-14014.	3.5	15
310	Square Grains in Asymmetric Rodâ^'Coil Block Copolymers. Langmuir, 2008, 24, 1604-1607.	3.5	15
311	Co3O4–Co2ZnO4 spinels: The case for a solid solution. Journal of Solid State Chemistry, 2012, 190, 143-149.	2.9	15
312	Dynamical Orientation of Large Molecules on Oxide Surfaces and its Implications for Dye-Sensitized Solar Cells. Chemistry of Materials, 2013, 25, 4354-4363.	6.7	15
313	Common Enzymological Experiments Allow Free Energy Profile Determination. Biochemistry, 2013, 52, 5952-5965.	2.5	15
314	Understanding the Selective Etching of Electrodeposited ZnO Nanorods. Langmuir, 2014, 30, 14079-14085.	3.5	15
315	Rapid thermal processing chamber for <i>in-situ</i> x-ray diffraction. Review of Scientific Instruments, 2015, 86, 013902. X-Ray Absorption Spectroscopy Study of Structure and Stability of Disordered	1.3	15
316	(Cu <inline-formula> <téx-math>\$_{f} Tj ETQq0 0 0 rgBT /Overlock 10 Tf 50 392 Td (2}\$<td>&gt;2.5</td><td>line-formula&amp; 15</td></téx-math></inline-formula>	>2.5	line-formula& 15
317	1-x}\$(ZnS) <inline-formula><tex-math>\$_{f} x}\$klt;/tex-math&gt; </tex-math></inline-formula> Alloys. IEEE Journal of Photovoltaics, 2015, 5, 372-377. Kinetic Versus Thermodynamic Orientational Preferences for a Series of Isomorphic Molecular Semiconductors. ACS Omega, 2018, 3, 10198-10204.	3.5	15
318	Acceptor Gradient Polymer Donors for Non-Fullerene Organic Solar Cells. Chemistry of Materials, 2019, 31, 9729-9741.	6.7	15
319	Impact of regioregularity on thin-film transistor and photovoltaic cell performances of pentacene-containing polymers. Journal of Materials Chemistry, 2012, 22, 4356.	6.7	14
320	Experimental Characterization of a Theoretically Designed Candidate p-Type Transparent Conducting Oxide: Li-Doped Cr <sub>2</sub> MnO <sub>4</sub> . Chemistry of Materials, 2014, 26, 4598-4604.	6.7	14
321	Conversion of Aminodeoxychorismate Synthase into Anthranilate Synthase with Janus Mutations: Mechanism of Pyruvate Elimination Catalyzed by Chorismate Enzymes. Biochemistry, 2015, 54, 2372-2384.	2.5	14
322	Directed evolution of the substrate specificity of dialkylglycine decarboxylase. Biochimica Et Biophysica Acta - Proteins and Proteomics, 2015, 1854, 146-155.	2.3	14
323	Extraordinarily Stable Amyloid Fibrils Engineered from Structurally Defined β-Solenoid Proteins. Biochemistry, 2017, 56, 6041-6050.	2.5	14
324	Controlling Polymer Morphology in Blade-Coated All-Polymer Solar Cells. Chemistry of Materials, 2021, 33, 5951-5961.	6.7	14

#	Article	IF	CITATIONS
325	Highly Reversible Plating/Stripping of Porous Zinc Anodes for Multivalent Zinc Batteries. Journal of the Electrochemical Society, 2020, 167, 140520.	2.9	14
326	Reticulated Organic Photovoltaics. Advanced Functional Materials, 2012, 22, 1167-1173.	14.9	13
327	Biological conversion of gaseous alkenes to liquid chemicals. Metabolic Engineering, 2016, 38, 98-104.	7.0	13
328	Graphene induced electrical percolation enables more efficient charge transport at a hybrid organic semiconductor/graphene interface. Physical Chemistry Chemical Physics, 2018, 20, 4422-4428.	2.8	13
329	Augmenting n-Type Performance of Ambipolar Top-Contact Organic Thin-Film Transistors by Self-Generated Interlayers. Chemistry of Materials, 2019, 31, 7046-7053.	6.7	13
330	Test of the Dynamic-Domain and Critical Scattering Hypotheses in Cubic Methylammonium Lead Triiodide. Physical Review Letters, 2020, 125, .	7.8	13
331	Using resonant energy X-ray diffraction to extract chemical order parameters in ternary semiconductors. Journal of Materials Chemistry C, 2020, 8, 4350-4356.	5.5	13
332	Electrochemical and electrochromic properties of nanoworm-shaped Ta2O5–Pt thin-films. Electrochemistry Communications, 2005, 7, 151-155.	4.7	12
333	In Situ Synchrotron X-ray Diffraction Experiments on Electrochemically Deposited ZnO Nanostructures. Journal of Physical Chemistry C, 2008, 112, 14863-14866.	3.1	12
334	In situ USAXS measurements of titania colloidal paint films during the drying process. Journal of Colloid and Interface Science, 2009, 336, 612-615.	9.4	12
335	Thermotropic Phase Transition of Benzodithiophene Copolymer Thin Films and Its Impact on Electrical and Photovoltaic Characteristics. Chemistry of Materials, 2015, 27, 1223-1232.	6.7	12
336	Li gradients for Li-rich cathodes. Nature Energy, 2019, 4, 1014-1015.	39.5	12
337	Analysis and Simulation of One-Dimensional Transport Models for Lithium Symmetric Cells. Journal of the Electrochemical Society, 2019, 166, A3806-A3819.	2.9	12
338	In Situ Characterization of Ferroelectric HfO <sub>2</sub> During Rapid Thermal Annealing. Physica Status Solidi - Rapid Research Letters, 2021, 15, 2000598.	2.4	12
339	Orientation-Dependent Distortion of Lamellae in a Block Copolymer Electrolyte under DC Polarization. Macromolecules, 2021, 54, 7808-7821.	4.8	12
340	Structure and Electrocatalysis of Sputtered RuPt Thin-Film Electrodes. Journal of Physical Chemistry B, 2005, 109, 12845-12849.	2.6	11
341	Correlation between luminescent properties and local coordination environment for erbium dopant in yttrium oxide nanotubes. Journal of Applied Physics, 2008, 103, 094316.	2.5	11
342	Simplified Models for Accelerated Structural Prediction of Conjugated Semiconducting Polymers. Journal of Physical Chemistry C, 2017, 121, 26528-26538.	3.1	11

#	Article	IF	CITATIONS
343	Hydrogen Purification in Palladium-Based Membranes: An Operando X-ray Diffraction Study. Industrial & Engineering Chemistry Research, 2019, 58, 926-934.	3.7	11
344	Surface equilibration mechanism controls the molecular packing of glassy molecular semiconductors at organic interfaces. Proceedings of the National Academy of Sciences of the United States of America, 2021, 118, .	7.1	11
345	Scattering techniques for mixed donor–acceptor characterization in organic photovoltaics. Materials Horizons, 2022, 9, 43-60.	12.2	11
346	Reduction of resistivity in Cu thin films by partial oxidation: Microstructural mechanisms. Applied Physics Letters, 2004, 84, 2518-2520.	3.3	10
347	Influence of Interfacial Layer Between Nanoparticles and Polymeric Matrix on Viscoelastic Properties of Hydrogel Nanocomposites. Macromolecules, 2009, 42, 1331-1343.	4.8	10
348	Absence of Mixed Phase in Organic Photovoltaic Active Layers Facilitates Use of Green Solvent Processing. Journal of Physical Chemistry C, 2018, 122, 11136-11144.	3.1	10
349	Effect of Molecular Shape on the Properties of Non-Fullerene Acceptors: Contrasting Calamitic Versus 3D Design Principles. ACS Applied Energy Materials, 2018, 1, 6513-6523.	5.1	10
350	Fullerene derivative induced morphology of bulk heterojunction blends: PIPCP:PC <sub>61</sub> BM. RSC Advances, 2019, 9, 4106-4112.	3.6	10
351	Bottom-up synthesis of protein-based nanomaterials from engineered β-solenoid proteins. PLoS ONE, 2020, 15, e0229319.	2.5	10
352	X-ray diffraction from anodic TiO2 films: in situ and ex situ comparison of the Ti (0001) face. Surface Science, 1994, 302, 341-349.	1.9	9
353	Local Atomic Structure of Partially Ordered NiMn in NiMn/NiFe Exchange Coupled Layers:Â 1. XAFS Measurements and Structural Refinement. Journal of Physical Chemistry B, 2005, 109, 10406-10418.	2.6	9
354	SAXSMorph: a program for generating representative morphologies for two-phase materials from small-angle X-ray and neutron scattering data. Journal of Applied Crystallography, 2011, 44, 221-224.	4.5	9
355	Vanadium As a Potential Membrane Material for Carbon Capture: Effects of Minor Flue Gas Species. Environmental Science & Technology, 2017, 51, 11459-11467.	10.0	9
356	Triptycene as a Supramolecular Additive in PTB7:PCBM Blends and Its Influence on Photovoltaic Properties. ACS Applied Materials & Interfaces, 2018, 10, 24665-24678.	8.0	9
357	Carbon Acidity in Enzyme Active Sites. Frontiers in Bioengineering and Biotechnology, 2019, 7, 25.	4.1	9
358	Combined Effects of Uniform Applied Pressure and Electrolyte Additives in Lithium-Metal Batteries. ACS Applied Energy Materials, 2022, 5, 8273-8281.	5.1	9
359	Nonequilibrium 2-Hydroxyoctadecanoic Acid Monolayers: Effect of Electrolytes. Langmuir, 2011, 27, 4430-4438.	3.5	8
360	Swelling of Polymer Dielectric Thin Films for Organic-Transistor-Based Aqueous Sensing Applications. Chemistry of Materials, 2013, 25, 5018-5022.	6.7	8

#	Article	IF	CITATIONS
361	Effects of aromatic regularity on the structure and conductivity of polyimideâ€poly(ethylene glycol) materials doped with ionic liquid. Journal of Polymer Science, Part B: Polymer Physics, 2015, 53, 509-521.	2.1	8
362	Unique Reversible Crystal-to-Crystal Phase Transition—Structural and Functional Properties of Fused Ladder Thienoarenes. Chemistry of Materials, 2017, 29, 7686-7696.	6.7	8
363	Improving molecular alignment and charge percolation in semiconducting polymer films with highly localized electronic states through tailored thermal annealing. Journal of Materials Chemistry C, 2021, 9, 15848-15857.	5.5	8
364	Vapor deposition rate modifies anisotropic glassy structure of an anthracene-based organic semiconductor. Journal of Chemical Physics, 2022, 156, 014504.	3.0	8
365	Revealing temperature-dependent polymer aggregation in solution with small-angle X-ray scattering. Journal of Materials Chemistry A, 2022, 10, 2096-2104.	10.3	8
366	Organic Solar Cells: How X-ray Scattering Has Improved Our Understanding of Morphology. Synchrotron Radiation News, 2010, 23, 16-21.	0.8	7
367	Evolution of nanoscale roughness in Cu/SiO2 and Cu/Ta interfaces. Applied Physics Letters, 2012, 100, 024106.	3.3	7
368	Controlling spin ordering in frustrated magnets via thin film heteroepitaxy. Physical Review B, 2012, 85, .	3.2	7
369	Site-directed mutant libraries for isolating minimal mutations yielding functional changes. Protein Engineering, Design and Selection, 2017, 30, 347-357.	2.1	7
370	High Tensile Strength of Engineered β-Solenoid Fibrils via Sonication and Pulling. Biophysical Journal, 2017, 113, 1945-1955.	0.5	7
371	Ptychography of Organic Thin Films at Soft X-ray Energies. Chemistry of Materials, 2019, 31, 4913-4918.	6.7	7
372	Kinetic origins of the metastable zone width in the manganese oxide Pourbaix diagram. Journal of Materials Chemistry A, 2021, 9, 7857-7867.	10.3	7
373	Interfacial effects in thin films of polymeric semiconductors. Journal of Vacuum Science & Technology B, 2008, 26, 1454.	1.3	6
374	Local Mechanical Perturbation Provides an Effective Means to Regulate the Growth and Assembly of Functional Peptide Fibrils. Small, 2016, 12, 6407-6415.	10.0	6
375	Synthesis and Crystallization of Atomic Layer Deposition β-Eucryptite LiAlSiO <sub>4</sub> Thin-Film Solid Electrolytes. ACS Applied Materials & Interfaces, 2020, 12, 56935-56942.	8.0	6
376	Twisted Aâ€Dâ€A Type Acceptors with Thermallyâ€Activated Delayed Crystallization Behavior for Efficient Nonfullerene Organic Solar Cells. Advanced Energy Materials, 0, , 2103957.	19.5	6
377	Why it is important to determine and report the impact of probe radiation. Joule, 2022, 6, 723-725.	24.0	6
378	Reaction-Mediated Transformation of Working Catalysts. ACS Catalysis, 2022, 12, 8007-8018.	11.2	6

#	Article	IF	CITATIONS
379	Magnetization profile in antiferromagnetically coupled recording media. Applied Physics Letters, 2005, 86, 162506.	3.3	5
380	In situevolution of stress gradients in Cu films induced by capping layers. Applied Physics Letters, 2010, 96, 261903.	3.3	5
381	Advanced X-ray Scattering and Spectroscopy Characterization of an Antisoiling Coating for Solar Module Glass. ACS Applied Energy Materials, 2019, 2, 7870-7878.	5.1	5
382	Manipulation and statistical analysis of the fluid flow of polymer semiconductor solutions during meniscus-guided coating. MRS Bulletin, 2021, 46, 380-393.	3.5	5
383	Reactive Vapor-Phase Additives toward Destabilizing γ-Mg(BH <sub>4</sub> ) <sub>2</sub> for Improved Hydrogen Release. ACS Applied Energy Materials, 2022, 5, 1690-1700.	5.1	5
384	Mitigating residual stress in Cu metallization. Applied Physics Letters, 2012, 101, 231906.	3.3	4
385	Effect of Extensional Flow on the Evaporative Assembly of a Donor–Acceptor Semiconducting Polymer. ACS Applied Electronic Materials, 2019, 1, 2445-2454.	4.3	4
386	Covalently Linked, Two-Dimensional Quantum Dot Assemblies. Langmuir, 2020, 36, 9944-9951.	3.5	4
387	Applications of synchrotron X-rays in microelectronics industry research. Nuclear Instruments & Methods in Physics Research B, 2005, 241, 247-252.	1.4	3
388	Microstructural origin of orientation ratio in magnetic recording media. Journal of Applied Physics, 2006, 99, 033907.	2.5	3
389	Effect of sintering conditions on mixed ionic-electronic conducting properties of silver sulfide nanoparticles. Journal of Applied Physics, 2012, 111, 053530.	2.5	3
390	Understanding stress gradients in microelectronic metallization. Powder Diffraction, 2012, 27, 92-98.	0.2	3
391	Understanding Cu incorporation in the <mml:math xmlns:mml="http://www.w3.org/1998/Math/MathML"&gt;<mml:mrow><mml:msub><mml:mi>Cu</mml:mi><mml:n structure using resonant x-ray diffraction. Physical Review Materials, 2021, 5, .</mml:n </mml:msub></mml:mrow></mml:math 	ח <b>ר∆⊮</b> > < mr	ml <b>:s</b> nn>2
392	Use of a Multiple Hydride Donor To Achieve an n-Doped Polymer with High Solvent Resistance. ACS Applied Materials & Interfaces, 2022, 14, 33598-33605.	8.0	3
393	Near-surface structure of aromatic polyimides: the effect of precursor isomers. Faraday Discussions, 1994, 98, 319.	3.2	2
394	Highly Regioselective Oneâ€Pot Synthesis of 7â€Hydroxyâ€6â€methylphthalide from 3â€Hydroxyâ€4â€methylbenzylalcohol. Synthetic Communications, 2005, 35, 2869-2874.	2.1	2
395	Microstructural effects on the performance of poly(thiophene) field-effect transistors. , 2006, 6336, 41.		2
396	Enrichment of Deuterium Oxide at Hydrophilic Interfaces in Aqueous Solutions. Langmuir, 2007, 23, 11943-11946.	3.5	2

#	Article	IF	CITATIONS
397	The Impact of the Dielectric/Semiconductor Interface on Microstructure and Charge Carrier Transport in High-Performance Polythiophene Transistors. ECS Transactions, 2008, 13, 113-122.	0.5	2
398	Preparation of crystalline dielectric modification silane layer by spin-coating and its improvements on organic transistor performance. Proceedings of SPIE, 2009, , .	0.8	2
399	Operando Transmission X-ray Microscopy Studies on Li-Ion Batteries. Microscopy and Microanalysis, 2014, 20, 1526-1527.	0.4	2
400	Tunable mesoscale-structured self-assembled hydrogels synthesized by organocatalytic ring-opening polymerization. Polymer, 2015, 65, 93-104.	3.8	2
401	<i>In silico</i> stress–strain measurements on self-assembled protein lattices. Soft Matter, 2018, 14, 8095-8104.	2.7	2
402	Thermodynamic guiding principles of high-capacity phase transformation materials for splitting H <sub>2</sub> O and CO <sub>2</sub> by thermochemical looping. Journal of Materials Chemistry A, 2022, 10, 3552-3561.	10.3	2
403	Light-induced halide segregation in perovskites with wrinkled morphology. Journal of Energy Chemistry, 2022, 71, 83-88.	12.9	2
404	High-resolution x-ray analysis of graphene grown on 4H–SiC (000) at low pressures. Journal of Materials Research, 2014, 29, 439-446.	2.6	1
405	A Novel Glutathione S-Transferase Gtt2 Class (VpGSTT2) Is Found in the Genome of the AHPND/EMS Vibrio parahaemolyticus Shrimp Pathogen. Toxins, 2021, 13, 664.	3.4	1
406	Multiple Hydrogen Transfers in Enzyme Action. , 0, , 1139-1170.		0
407	Relating microstructure to transport in organic semiconductor transistors. , 2009, , .		0
408	A crystalline alkylsilane dielectric surface-modification layer: a general strategy for high performance organic thin-film transistors. Proceedings of SPIE, 2009, , .	0.8	0
409	Al tool makes phase identification crystal clear. Nature Computational Science, 2021, 1, 311-312.	8.0	0
410	Manipulation and statistical analysis of the fluid flow of polymer semiconductor solutions during meniscus-guided coating. MRS Bulletin, 0, , 1-14.	3.5	0
411	Increased crystallite size in thin films of C <sub>60</sub> and <i>p</i> -terphenyls <i>via</i> PDMS-assisted crystallization. Journal of Materials Chemistry C, 2022, 10, 5657-5665.	5.5	0